Advanced Ceramics Progress: Vol. 10, No. 4, (Autumn 2024) 5-14

Materials and Energy Research Center
MERC

Contents lists available at ACERP

Advanced Ceramics Progress

Journal Homepage: www.acerp.ir

Original Research Article

Exploring the Potential of ZnS/CdS Dual Nanocomposites in Photocatalytic Degradation for Water Cleanup

Amir Hossein Afzali [a], Maryam Hajiebrahimi [b], Mohammad Mahdi Hosseinieh Farahani [a], Sanaz Alamdari [c], Omid Mirzaee [d]*

[a] *BSc Student, Faculty of Materials and Metallurgical Engineering, University of Semnan, Iran.*
[b] *Research Assistant, Faculty of Materials and Metallurgical Engineering, University of Semnan, Iran.*
[c] *Assistant Professor, Department of Nanotechnology, Faculty of New Sciences and Technologies, University of Semnan, Iran.*
[d] *Professor, Faculty of Materials & Metallurgical Engineering, University of Semnan, Iran.*

* Corresponding Author Email: o_mirzaee@semnan.ac.ir (O. Mirzaee)
URL: https://www.acerp.ir/article_214778.html

ARTICLE INFO

Article History:
Received: 04 November 2024
Revised: 04 November 2024
Accepted: 21 December 2024

Keywords:
ZnS/CdS,
Solvothermal,
Nanocomposite,
Band Gap,
Photocatalysis

ABSTRACT

The use of photocatalytic degradation to address environmental cleanup issues is gaining popularity. In this work, pure ZnS, CdS, and ZnS/CdS heterostructure nanocomposites with superior photocatalyst efficiency were synthesized using a straightforward coprecipitation technique and a solvothermal process. The structural, morphological, and optical characteristics were analyzed using XRD, EDX, FTIR, FESEM, and UV-Vis absorbance measurement techniques. The XRD data indicated that ZnS/CdS nanocomposites were produced with an average crystallite size of 15–20 nm. The UV-Vis measurements revealed an optical band gap ranging from 4.4 eV to 5.3 eV. The photocatalytic efficacy of the ZnS/CdS heterostructure nanocomposites in degrading methylene blue (MB) dye was evaluated under UVA light. The synthesized ZnS/CdS nanocomposite exhibited remarkable decolorization efficiency (99%) within just 5 minutes of UVA light exposure. This straightforward method has the potential to be scaled up for industrial applications.

https://doi.org/10.30501/acp.2025.486343.1165

1. INTRODUCTION

Most of the world's freshwater supplies are being depleted due to deforestation and the rapid growth of urbanization, transportation, and industry (Suárez et al, 2018). Consequently, one of the most pressing issues faced by both industrialized and developing nations is water scarcity (Suárez et al, 2018; Soltani et al, 2012). Wastewater can be treated using a variety of techniques, though many of these have limitations. Water treatment primarily involves physical, chemical, and biological processes (Yuan et al, 2018; Chen et al, 2015). Among the most notable techniques is the advanced oxidation process (AOP), which can eliminate organic and hazardous pollutants as well as natural toxins, dyes, pesticides, and other harmful substances. Photocatalysis, a leading advanced oxidation process (AOP) in recent years, has garnered significant interest as a cost-effective and eco-friendly method for cleaning water sources (Mumin et al, 2015). Various types of semiconductor photocatalysts have been developed, including single, doped, and coupled semiconductor (heterostructure) photocatalysts (Zhang et al, 2017). To reduce the recombination of photogenerated electron-hole pairs, enhance photocatalytic activity, narrow the band gap, and shift optical sensitivity into the visible range, combining semiconductors with different energy levels presents an

Please cite this article as: Afzali, A. H., Hajiebrahimi, M., Hosseinieh Farahani, M. M., Alamdari, S. & Mirzaee, O. (2024). Exploring the Potential of ZnS/CdS Dual Nanocomposites in Photocatalytic Degradation for Water Cleanup. *Advanced Ceramics Progress*. 10(4), 5-14. https://doi.org/10.30501/acp.2025.486343.1165

exciting and effective strategy (Zhai et al, 2015). Deforestation, rapid urbanization, transportation, and industrial activities are major contributors to the depletion of the world's freshwater resources (Li et al, 2017). As a result, water scarcity has become one of the most critical challenges for both developed and developing nations (Yuan et al, 2018). Numerous methods for wastewater treatment exist, yet many have shortcomings. The main methods employed in water treatment include physical, chemical, and biological processes (Esparza et al, 2017). Among these, the advanced oxidation process (AOP) stands out as a remarkable approach capable of removing organic and toxic pollutants, natural toxins, pesticides, dyes, and other hazardous materials (Reiss et al, 2009). Researchers have shown a growing interest in coupled or heterostructure photocatalysts, making this an exciting and rapidly evolving area of study (Li et al, 2011; Malik, 2002). Photocatalysis has emerged as one of the most promising AOPs in recent years, attracting significant attention for its environmentally friendly applications. ZnS is highly responsive to UV light, making it one of the most efficient inorganic photocatalysts. Its low cost, chemical stability, and ease of large-scale production make ZnS nanostructures especially desirable for photocatalytic applications (Schattka et al, 2002; Yang et al, 2005). The physicochemical properties of metal oxide nanoparticles are further enhanced through doping. Numerous ZnS-based coupled oxide semiconductor nanomaterials, such as TiO2/ZnS, CuO-ZnS, Fe_2O_3/ZnS, WO_3/ZnS, and CdS/ZnS, have been developed to degrade organic contaminants. However, to the best of our knowledge, PWO/ZnS heterostructures have rarely been explored (Li et al, 2009).

When selecting semiconductor materials, several factors must be considered (Zhang et al, 2019). Metal oxide and sulfide semiconductors have attracted considerable interest in semiconducting-based photodegradation due to their high synthesis temperature requirements. One key advantage of metal sulfides, however, is that they can be synthesized under ambient conditions (Pei et al, 2019). Moreover, the reduced water solubility of metal sulfides minimizes secondary contamination and metal cation leaching. For these reasons, ZnS was chosen for this study (Zhou et al, 2020).

In this work, ZnS/CdS dual nanocomposites were synthesized using the co-precipitation method. Structural and morphological analyses confirmed the successful incorporation of CdS and ZnS nanoparticles. Most notably, the resulting composite demonstrated excellent photocatalytic activity and efficient dye degradation (e.g., methylene blue), offering broad potential applications in water treatment.

2. MATERIALS AND METHODS

2.1. Materials

All chemical precursors were employed without further purification because they were of analytical purity. Sodium sulfide ($Na_2S.9H_2O$), zinc acetate dihydrate (Zn $(CH_3CO_2)_2.2H_2O$) (99.9%), and cadmium acetate dihydrate (Cd $(CH_3COO)_2.2H_2O$) were purchased from Sigma-Aldrich. Ethanol and deionized water were used to prepare aqueous solutions.

2.2. Synthesize of ZnS and CdS nanoparticles

Zinc sulfide (ZnS) is typically synthesized by dissolving zinc acetate and sodium sulfide in 50 milliliters of deionized water, a process known as the preparation of ZnS NPs (Afzali et al, 2024; Farahani et al, 2024). Subsequently, sodium sulfide solution is cautiously added to the zinc acetate solution using the coprecipitation method. The resulting solution underwent three centrifugation cycles and was then dried for 24 hours at 80 °C. Ultimately, the sample was placed in a furnace and heated to 800 °C for one hour to produce zinc sulfide powder. Similarly, the coprecipitation technique was employed to synthesize CdS NPs. Cadmium acetate dihydrate and sodium sulfide were dissolved in deionized water in an equal molar ratio.

The cadmium acetate solution was then mixed with the $Na_2S{\cdot}9H_2O$ solution. The resulting precipitate was cleaned, centrifuged, and dried for 24 hours at 80 °C. As the final step, the sample was calcined at 600 °C for 2 hours.

2.3. Synthesize of ZnS/CdS nanocomposite

The ZnS/CdS nanocomposite was synthesized via sonication and solvothermal methods. ZnS and CdS were combined in 20 milliliters of ethanol at a 1:1 molar ratio. After being dissolved using a magnetic stirrer, the resulting solution was placed in an ultrasonic bath for 15 minutes. The slurry was then transferred to a PTFE-lined autoclave and heated to 110 °C. After 12 hours, the resulting solution was centrifuged, cleaned, and oven-dried (Hajiebrahimi et al, 2024). The experimental process for preparing the ZnS/CdS nanocomposite is demonstrated in Figure 1.

2.4. Characterization

FTIR, UV-Vis, XRD, EDX-Mapping, and FESEM were used to examine the prepared sample. The crystal structure of the nanopowder was investigated using a Panalytical X-ray diffractometer with Cu Kα radiation (λ = 0.154 nm). FTIR spectra of the ZnS/CdS composite were obtained using a Perkin-Elmer Model 1800 spectrometer. The morphology of the resulting powder and composite was analyzed using a FESEM (MIRA3 TESCAN-XMU) (Yang et al, 2005). Transmission spectra of the samples were measured in the 200–900 nm wavelength range using a UV-Vis spectrophotometer (LAMBDA-PerkinElmer).

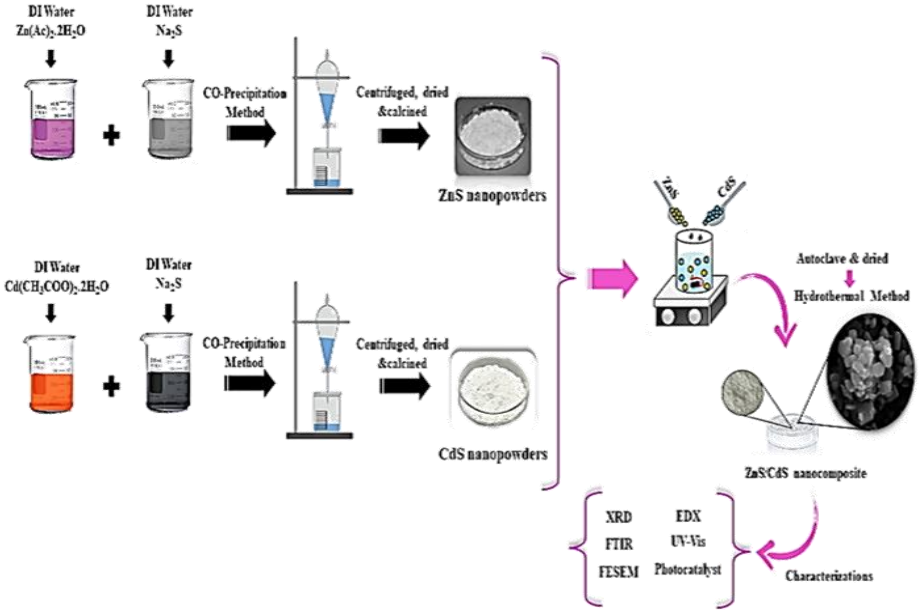

Figure 1. Experimental process and characterization method

2.5. Photocatalytic experiments

The photocatalytic performance of the samples was examined under UVA light at room temperature using MO as water pollutants. For this purpose, an appropriate amount of sample was added to a 20 mL contaminated solution (10 ppm MB). The distance between the aqueous solutions and the UV light source was maintained at 20 cm. To achieve adsorption/desorption equilibrium, the solution was vigorously magnetically stirred for 20 minutes prior to light irradiation. Following this, the light was turned on, and the solutions were continuously stirred. A 5 mL of the solution was removed from the suspension at 5-minute intervals, and the catalyst particles were settled down by centrifuging the mixture at 5000 rpm. The degradation of dye concentration was analyzed using a UV-Vis spectrophotometer, and UV-visible absorption spectra were recorded.

The following Equation (1) estimates the percentage of dye removal and decolorization efficiency, where C_0 (mg/l) is the initial dye concentration, and C_t (mg/l) the dye concentration at time t.

$$(\%) = \frac{C_0 - C_t}{C_0} \times 100 \quad (1)$$

3. Results and discussion

3.1. XRD

XRD was employed to investigate the structural features of the ZnS nanoparticles. As seen in Figure 2. The hexagonal structural arrangement in the pure ZnS sample is represented by the peaks observed at 26.94, 28.49, 30.55, 39.61, 47.59, 51.76, 55.54, 56.41, 57.62, 63.59, 72.94, and 76.1. The crystallographic planes corresponding to these points are (100), (002), (101), (102), (110), (103), (200), (112), (201), (202), (203), and (210), respectively. The hexagonal wurtzite phase is the bulk ZnS polymorph that is thermodynamically stable at ambient temperature. The crystal lattice constants, namely a = 0.382 and c = 0.626, closely match the standard diffraction pattern shown on the reference card (JCPDS card no. 96-901-3413). It is noteworthy that the highest intensity peak, which exceeds the intensity of any other peak, resluts from the incremental growth in the (002) crystallographic direction (Li et al, 2013). The diffraction peaks for pure CdS can only be indexed through its hexagonal structure, which aligns with the published data (JCPDS card no. 01-077-2306). In the pure CdS, a strong triplet peak is observed at planes (100), (002), and (101). At 2θ=25.36º, 26.12º, 28.37º, 36.24º, 45.06º, 49.83º, 52.46º, 53.64º, 55.38º, 60.27º, 66.63º, 70.42º, and 76.85º, the hexagonal phase of CdS peaks correspond to the crystal planes (100), (002), (101), (102), (200), (112), (004), (202), (203), (210), (211), and (105), respectively (Madhavi et al, 2021).

As seen in Figure 2, the XRD pattern of ZnS/CdS nanocomposites demonstrates the simultaneous presence of ZnS and CdS phases. The nanocomposites comprised hexagonal ZnS and CdS, and no more impurity peaks were visible in the diffractograms. The peaks for ZnS and CdS are sharp. The average crystallite size of the nanocomposite was also calculated using the Debye-Scherrer formula, $D = 0.9\lambda/\beta\cos\theta$, where θ is the diffraction angle, λ = 1.5406 Å, and β is the peak width at half maximum intensity (Alamdari et al, 2022; Hajiebrahimi et al, 2022). The crystallite size was found to rangebetween 15.88 and 16.87 nm. Table 1 provides information on the structural parameters (Li et al, 2009).

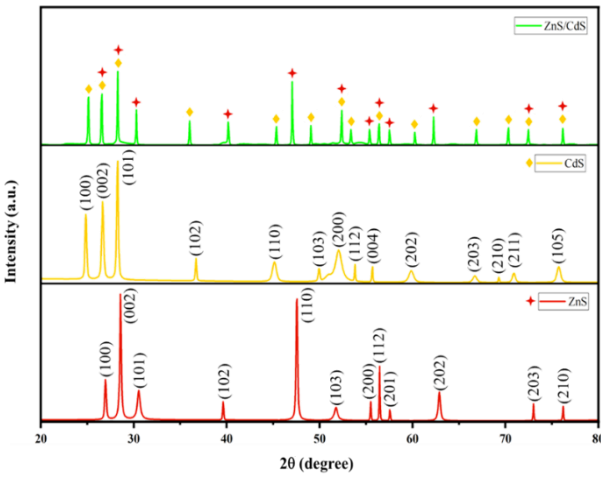

Figure 2. XRD patterns of pure ZnS, CdS, and CdS/ZnS nanocomposites.

TABLE 1. Measurements of crystallite size of samples.

Sample	Peak position	FWHM	D(nm)
ZnS	28.4923	0.1652	54.91
CdS	28.3754	0.1830	47.10
ZnS/CdS	28.2696	0.0900	15.88

3.2. FTIR

The chemical bonds of the synthesized semiconductors were assessed, and the organic species required for the synthesis processes were identified in the sample using FT-IR spectroscopy. Figure 3 displays the acquired spectra. Utilizing FT-IR for CdS, the existence of functional groups was confirmed, revealing O–H, C=C, and C–O functional group stretching and bending vibrations. A significant peak at 3440.77 cm−1, assigned to O–H, indicates that water has an affinity for CdS, while peaks at 1108.99 cm−1 and 1068.49 cm−1 correspond to the C–O and C=C stretching modes of carbonyl and carboxyl groups, respectively. The Cd–S bond exhibits an absorption band in the CdS spectrum at approximately 621.04 cm−1, whereas the –CS2 wagging is associated with the band at about 599.82 cm−1. The presence of the Cd–S bond is further confirmed by a peak detected at 447.45 cm−1. Peaks observed at 526.53 cm−1 are allocated to the metal-sulfur bond region, indicating the formation of Cd–S bonds. Figure 3 also illustrates the FT-IR transmittance spectrum of the synthesized ZnS nanoparticles. The ZnS nanoparticles exhibit peaks corresponding to ZnS, confirming the production of high-quality products. Several peaks at 3446.56, 1218.93, and 453.24 cm−1 are visible in the FT-IR spectra (Figure 3). The broad, weak peak at 3446.56 cm−1 is attributed to the stretching and bending modes of small amounts of adsorbed water on the particles. The peak at 1218.93 cm−1 is associated with nitrate groups, while the peak at 453.24 cm−1 corresponds to cubic ZnS, linked to Zn–S vibrations (Yuan et al, 2018). The FT-IR spectra validated the materials' composition and purity. The various peaks produced by the samples provide insight into the FT-IR spectra. The absorption peak in the region of 3600 to 3400 cm−1 represents the –OH group of water adsorbed by the samples. A weak absorption band at 1633.59 cm−1 is attributed to CO2 adsorbed on the particle surface, which is typical for high-surface-area nanoparticle powders (Mangla et al, 2019). The –OH mode of the water molecule is responsible for the band observed at 1108.99 cm−1, while the band located at 1456.16 cm−1 indicates the O–H stretching vibration mode. The metal-sulfide bond (Cd–S) is recognized by the band at 480.24 cm−1. Similarly, the bands observed at 603.68 cm−1 and 898.77 cm−1 are attributed to the stretching of zinc and sulfide and the metallic bond of Zn-S.

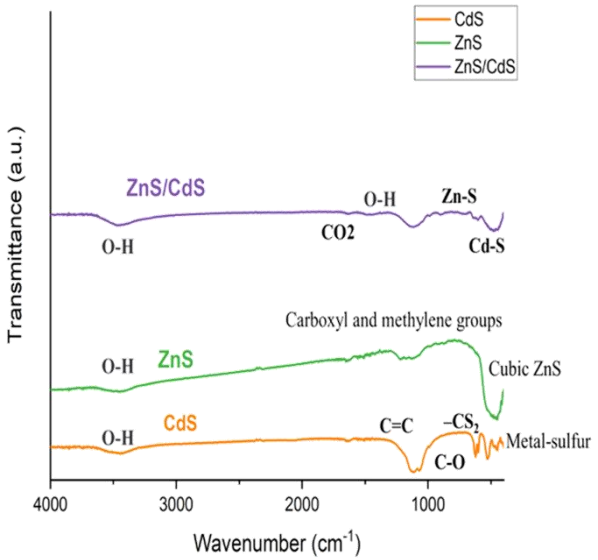

Figure 3. FT-IR spectrum of ZnS, CdS, and ZnS/CdS nanocomposite.

3.3. FESEM and EDX

The synthesized ZnS, CdS, and ZnS/CdS nanocomposite FESEM images are displayed in Figure 4(a, b, and c). FESEM was employed to analyze the shapes of the materials. The size and morphology of the ZnS microstructure were first assessed using SEM, with Figure 4(a) showing FESEM images that capture the unique structure of ZnS. Each sample exhibits a consistent spherical or semi-spherical structure with a diameter of 1–2 μm, as shown in Figure 4(a). Occasionally, two spheres were observed to come together. As seen in Figure 4(a), the ZnS nanoparticles display a similar elliptical shape with a particle size of approximately 159 nm (Kannan et al, 2020).

The FESEM images of the synthesized CdS nanoparticles are shown in Figure 4(b). The images reveal the spherical and semi-spherical morphologies of the CdS nanopowders synthesized via co-precipitation.

As shown in Figure 4(b), the CdS nanopowders exhibit an elliptical shape with a particle size of approximately 95 nm (Kim et al, 2007).

As seen in Figure 4(c), the ZnS/CdS nanocomposites have particles with an elliptical shape and a size of approximately 189 nm (El-Bially et al, 2012).

Elemental mapping and EDX were employed to evaluate the surface element distribution and composition of the synthesized nanocomposites. The EDX spectrum of the ZnS/CdS nanocomposite, as seen in Table 2, indicates that Zn, Cd, and S are present in the finished product. The elemental mapping of the nanocomposites' color composition is shown in Figure 5(a–e). Zn, Cd, and S are uniformly distributed throughout the nanocomposite material, as seen in Figure 5(a–e) (Zhang et al, 2004).

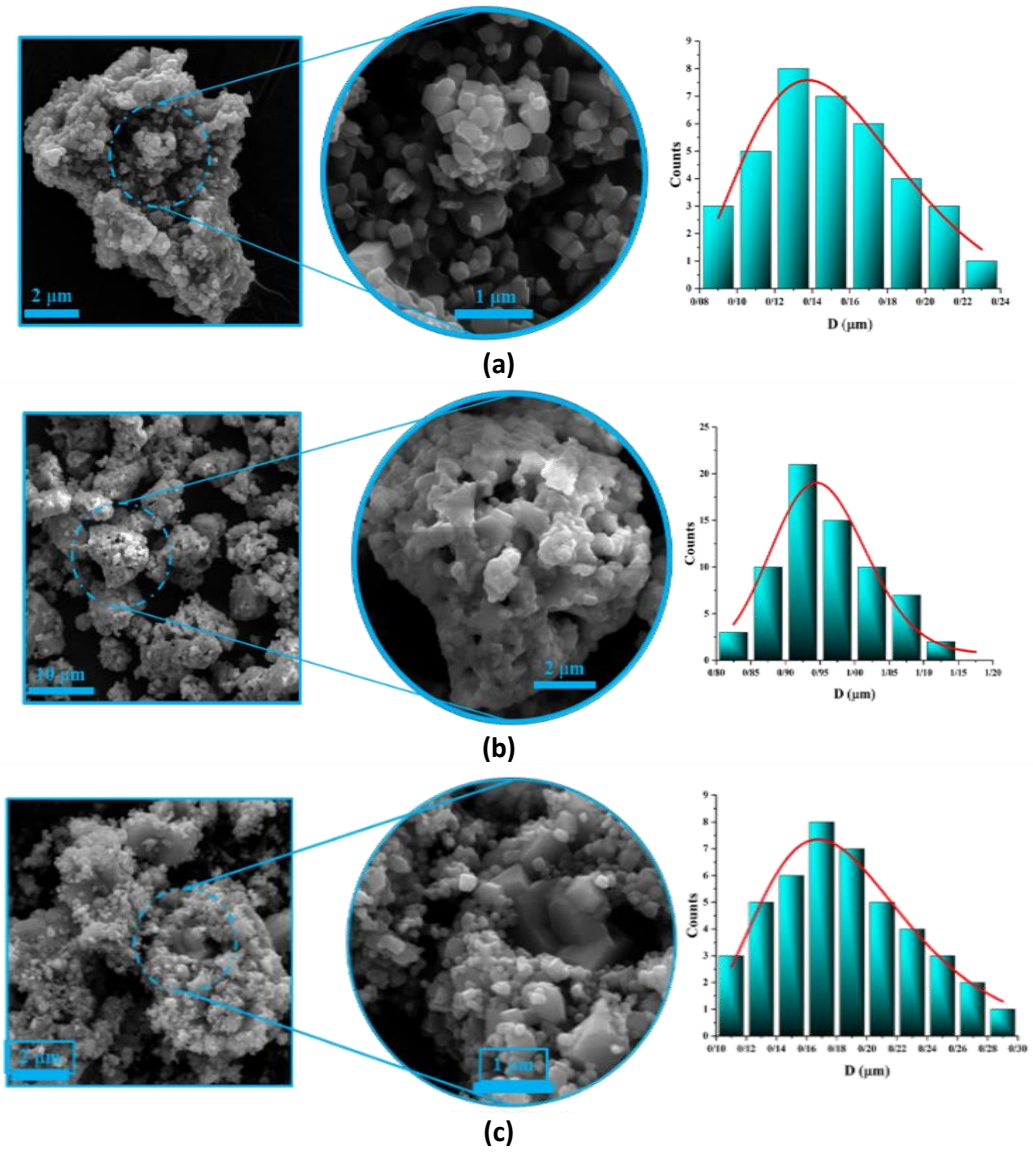

Figure 4. FESEM images of (a) pure ZnS, (b) pure CdS, and (c) ZnS/CdS nanocomposite.

TABLE 2. Measurements of crystallite size of samples.

Element	Wt%	Atomic %
O	25.02	60.4
S	3.95	4.75
Zn	42.13	24.89
Cd	27.35	9.4
Total:	100	100

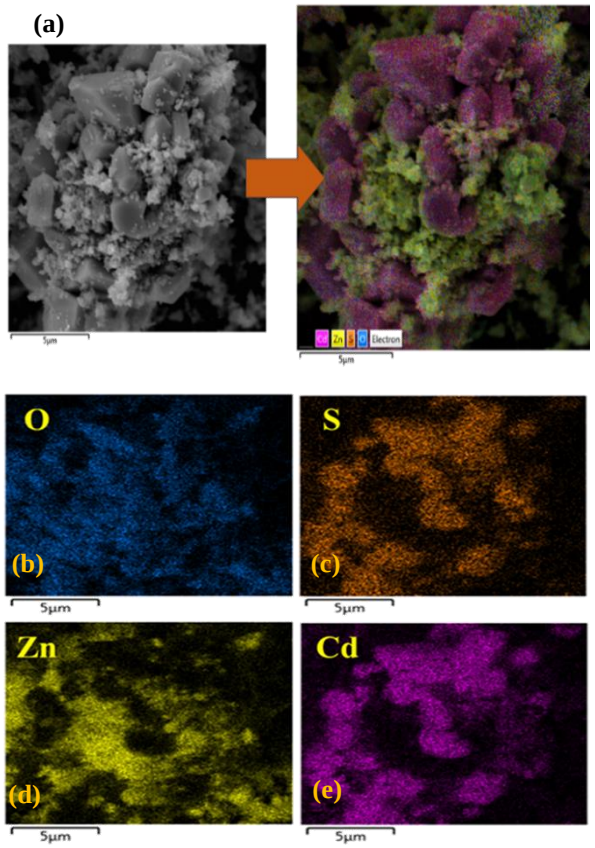

Figure 5. (a) Map elemental of the combine, (b) O, (c) S, (d) Zn, and (e) Cd, elements of ZnS/CdS nanocomposite.

3.4. Ultraviolet-visible (UV-Vis)

The optical absorption and bandgap studies of the nanoparticles were carried out using the diffuse reflectance spectra of ZnS and CdS, as shown in Figure 6(a) and (b). Plank's equation, $\alpha hv=A(hv-Eg)^n$, was used to evaluate the synthesized catalysts' bandgap properties (Hajiebrahimi et al, 2025) The UV-vis absorption spectra were utilized to measure the wavelength at which the samples absorbed the most light. The optical absorption margins for CdS and ZnS were found to be between 251–558 nm and 250–430 nm, respectively (Figure 7). The synthesized ZnS and CdS optical bandgaps were measured to be 4.46 eV and 5.36 eV, respectively, as shown in Figure 7(a) and (b). These estimated bandgaps are larger than those of their bulk counterparts. This bandgap widening can be attributed to the larger synthetic materials and the quantum confinement effect in the nanoparticles. The UV-vis absorption spectrum analysis demonstrates that the synthesized materials are capable of absorbing light in the visible and near-infrared regions of the electromagnetic spectrum. Due to their significant absorption in the visible region, it can be concluded that the synthesized materials are predictably photocatalytically active when exposed to visible light (El-Bially et al, 2012).

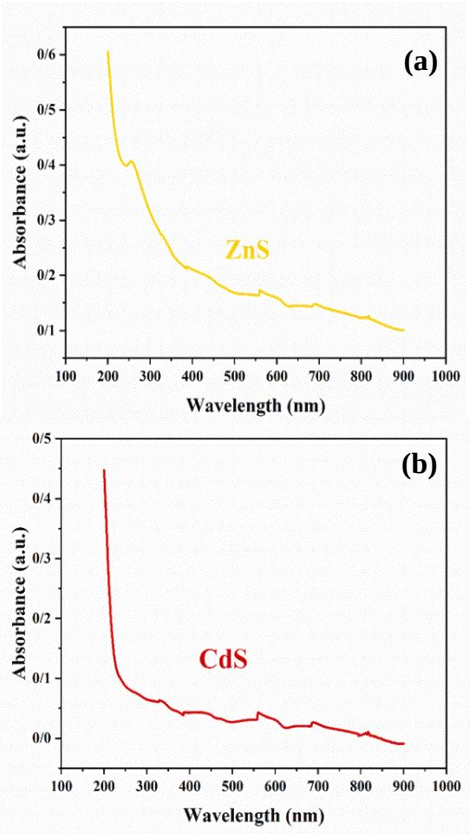

Figure 6. UV–vis spectra of ZnS (a) and CdS (b) samples.

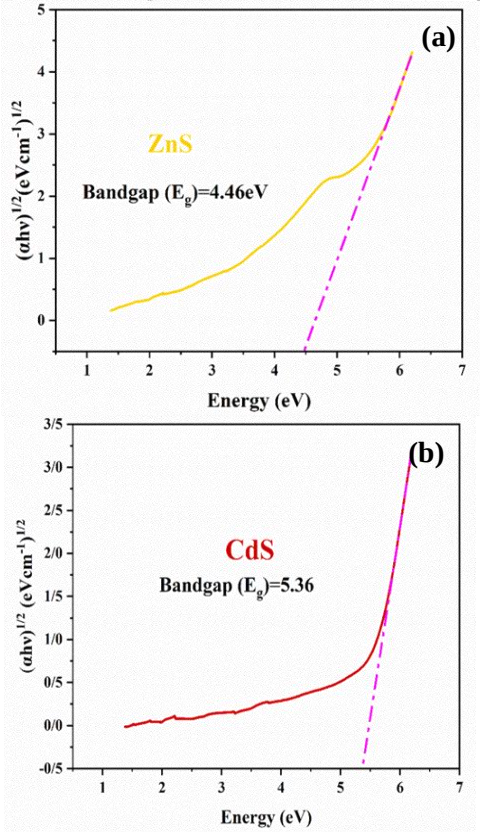

Figure 7. Corresponding Tauck's plots of ZnS (a) and CdS samples (b).

Figure 8a shows the UV-Vis spectrum of the CdS/ZnS nanocomposite sample. This sample absorbs light in both the visible and UV spectra. Its good optical absorption properties are indicated by the significant absorption of light below 550 nm (Afzali et al, 2024). It is therefore expected that the dual semiconductor system would play a major role in photocatalysis. The $(Ahv)^{1/2}$ versus hv curves, shown in Figure 8b, can be used to calculate the sample's band gap (Eg). The values of A, h, and ν represent the absorption ratio, Planck's constant, and light frequency, respectively (Amma et al, 2008). The band gap of the CdS/ZnS sample is determined to be 5.12 eV. Pure CdS has a band gap of 5.36 eV, as previously demonstrated, while ZnS has a band gap of 4.46 eV. In comparison to ZnS and CdS, the samples exhibit a red shift. As the concentration of CdS in CdS/ZnS nanocomposites increases, the samples also show an increase in crystal defects. A red shift and band gap narrowing occur in the UV-Vis spectrum (Estévez-Hernández et al, 2012).

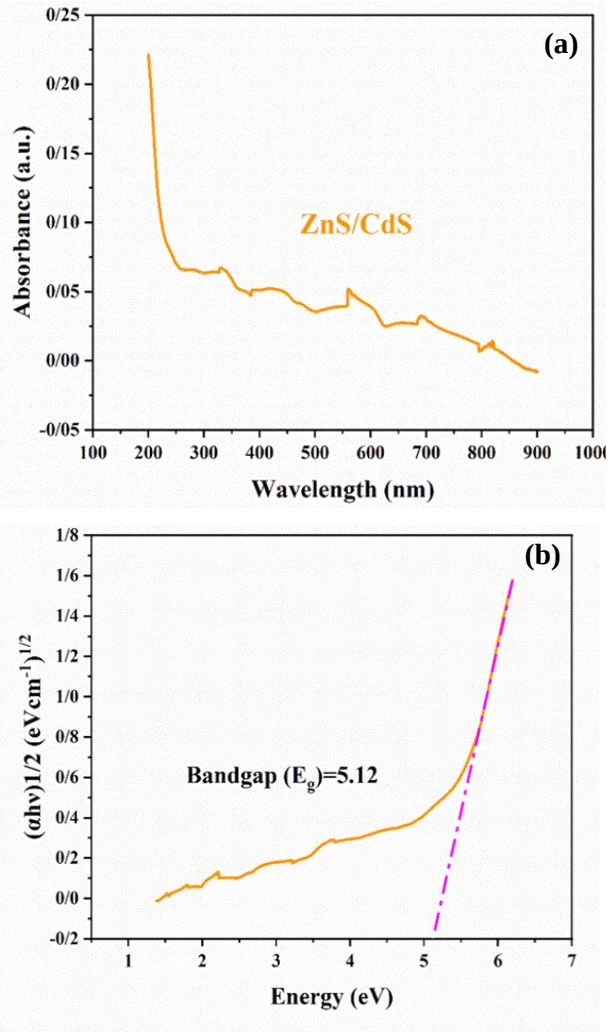

Figure 8. UV–vis spectra of ZnS/CdS (a) and $(\alpha hv)^{1/2}$ vs. photon energy (hv) for ZnS/CdS nanoparticles (b).

3.5. Photocatalytic activity

Evaluating the materials' photocatalytic activity involved tracking the rate at which the methylene blue dye in an aqueous solution degraded under UVA light irradiation (UVA 250W). 0.005 grams of each sample were individually dissolved in blue-colored solutions with a concentration of CO = 0.020g/L at neutral pH to evaluate the photocatalytic degradation performance of the synthesized materials. The resultant solutions were then separately mixed with the appropriate volume. The first 50 ml sample was positioned 20 cm away from the UV light. It should be noted that, to establish absorption/desorption equilibrium, the solutions were stirred rapidly for 15 minutes prior to light irradiation. After that, the UV light was switched on, and 5 ml portions of the zinc sulfide, cadmium sulfide, and nanocomposite solutions were removed from the mother solution at intervals of 5 minutes, 10 minutes, and 5000 rpm while the solutions were still being stirred. The samples were then centrifuged and analyzed using UV-Vis spectroscopy (Shuai et al, 2011).

The UV-Vis absorption spectra of the methylene blue solution, which was catalyzed by the synthesized materials, are displayed in Figures 9(a-c). The absorption intensity of methylene blue decreased with increasing reaction time when the solutions were exposed to radiation for 35 minutes for zinc sulfide, 60 minutes for cadmium sulfide, and 5 minutes for the nanocomposite. This decrease suggests that both pure samples and composite samples effectively broke down the organic dyes in the aqueous solution (Nizamoglu et al, 2007).

The synthesized samples' photocatalytic breakdown of methylene blue is depicted in Figure 10(a-c). These findings demonstrate that, in contrast to earlier research, we were able to achieve better photocatalytic degradation efficiency for the pure ZnS sample. In just 35 minutes, we attained a degradation level of over 95%. The photocatalytic efficiency of the pure CdS sample was around 60%, much lower than that of the pure ZnS and nanocomposite samples. In other words, the nanocomposite's photocatalytic efficacy significantly improved, resulting in almost 100% color deterioration. This improvement in photocatalytic degradation performance may be attributed to the proper rearrangement of energy levels resulting from the two semiconductors being closely and properly connected. This link has benefited charge transport between the valence and conduction bands at the interface of the two semiconductors. Since this connection helps prevent the electron-hole pair from recombining quickly, it facilitates the movement of these charge carriers to the surface, where they can react with the absorbed reactive species (Luo et al, 2019).

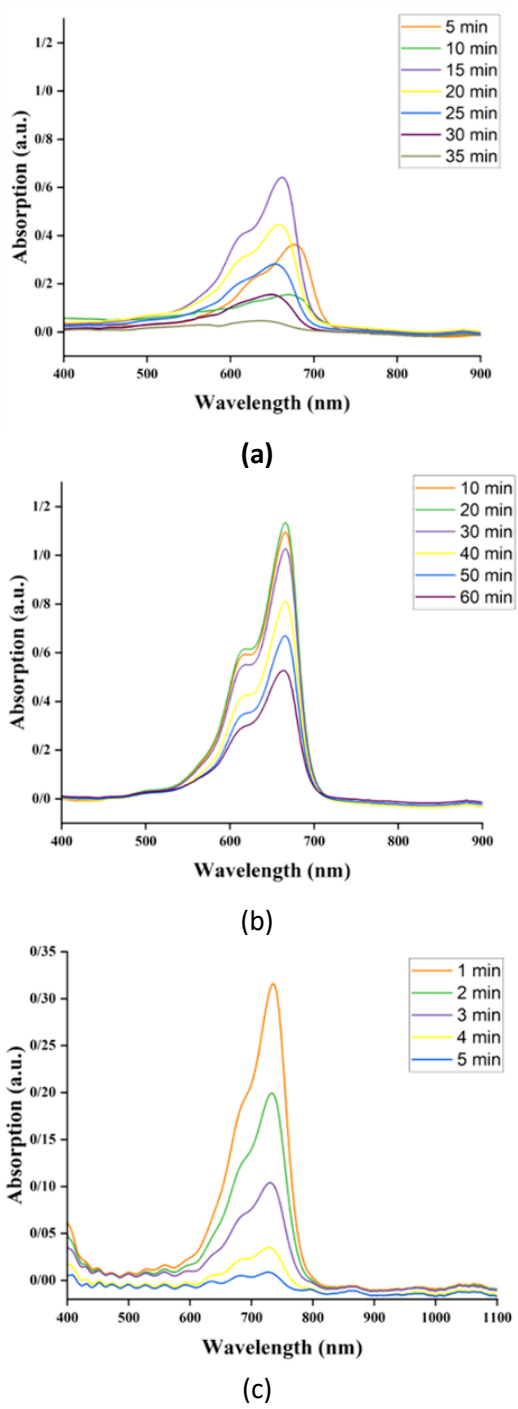

Figure 9. UV-Vis absorption spectrum of methylene blue solution catalyzed by the synthesized samples: a) ZnS, b) CdS, and c) ZnS/CdS nanocomposite.

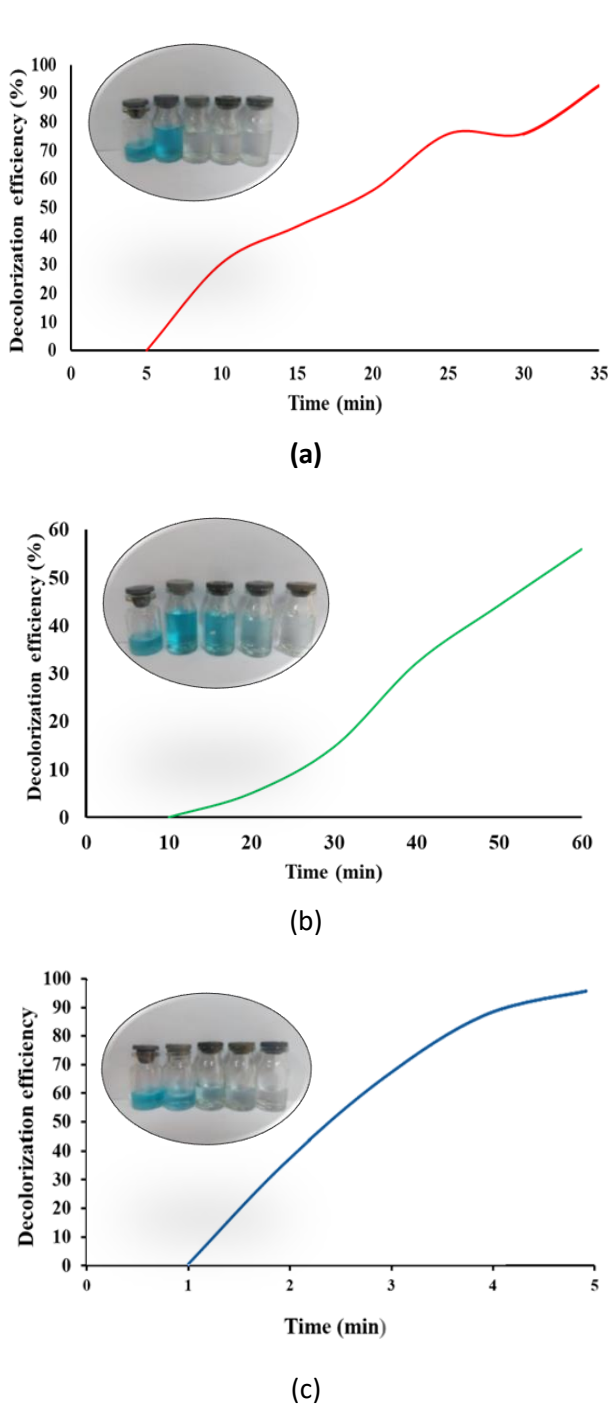

Figure 10. Comparison of decolorization performance of a: ZnS, b: CdS, and c: ZnS/CdS nanocomposite under UV light irradiation.

4. Conclusion

In summary, the solvothermal method proved effective for synthesizing CdS/ZnS dual nanocomposites. Comprehensive characterizations and tests were performed to evaluate the impact of combining ZnS and CdS on the photocatalytic activity of the CdS/ZnS dual nanocomposites. Among the samples produced, the nanocomposite exhibited the highest photocatalytic performance, achieving 99% methylene blue (MB) degradation efficiency within approximately five minutes. This high degradation rate highlights the material's potential for applications in environmental remediation and water purification.

ACKNOWLEDGEMENTS

The authors wish to acknowledge Semnan University for all the support throughout this work.

REFERENCES

1. Afzali, A. H., Seddiqi, A., Akbari, Z., Hajiebrahimi, M., Alamdari, S., & Mirzaee, O. (2024). Synthesis and characterization of ZnS and Ag-ZnS nanoparticles for photocatalytic degradation of aqueous pollutants. Synthesis and Sintering, 4(4), 248-255. https://doi.org/10.53063/synsint.2024.44258
2. Alamdari, S., Haji Ebrahimi, M., Mirzaee, O., Jafar Tafreshi, M., Majlesara, M. H., Tajally, M., ... & Mohammadi, A. (2022). Cerium doped tungsten-based compounds for thermoluminescence application. Progress in Physics of Applied Materials, 2(1), 35-40. https://doi.org/10.22075/ppam.2022.27086.1028.
3. Amma, B. S., Manzoor, K., Ramakrishna, K., & Pattabi, M. (2008). Synthesis and optical properties of CdS/ZnS coreshell nanoparticles. Materials Chemistry and Physics, 112(3), 789-792. https://doi.org/10.1016/j.matchemphys.2008.06.043
4. Chen, X., Lin, P., Yan, X., Bai, Z., Yuan, H., Shen, Y., ... & Zhang, Y. (2015). Three-dimensional ordered ZnO/Cu2O nanoheterojunctions for efficient metal–oxide solar cells. ACS applied materials & interfaces, 7(5), 3216-3223. https://doi.org/10.1021/am507836v
5. El-Bially, A. B., Seoudi, R., Eisa, W., Shabaka, A. A., Abd El-Hamid, R. K., & Ramadan, R. A. (2012). Preparation, characterization and physical properties of CdS nanoparticles with different sizes. Journal of Applied Sciences Research, 8(2), 676-685. https://www.researchgate.net/publication/259327880
6. Esparza, D., Lopez-Luke, T., Oliva, J., Cerdán-Pasarán, A., Martínez-Benítez, A., Mora-Seró, I., & De la Rosa, E. (2017). Enhancement of efficiency in quantum dot sensitized solar cells based on CdS/CdSe/CdSeTe heterostructure by improving the light absorption in the VIS-NIR region. Electrochimica Acta, 247, 899-909. https://doi.org/10.1016/j.electacta.2017.07.060
7. Estévez-Hernández, O., González, J., Guzmán, J., Santiago-Jacinto, P., Rendón, L., Montes, E., & Reguera, E. (2012). Mercaptopropionic Acid Capped CdS@ ZnS Nanocomposites: Interface Structure and Related Optical Properties. Science of Advanced Materials, 4(7), 771-779. https://doi.org/10.1166/sam.2012.1372
8. Farahani, M. M. H., Hajiebrahimi, M., Alamdari, S., Najafzadehkhoee, A., Khounsaraki, G. M., Agheb, M., ... & Mirzaee, O. (2024). Synthesis and antibacterial activity of silver doped zinc sulfide/chitosan bionanocomposites: A new frontier in biomedical applications. International Journal of Biological Macromolecules, 280, 135934. https://doi.org/10.1016/j.ijbiomac.2024.135934
9. Hajiebrahimi, M., Alamdari, S., & Mirzaee, O. (2024). The Potential of Silver-Doped Zinc Sulfide/Cadmium Sulfide Nanocomposites in Optoelectronic Applications. *Iranian Journal of Materials Science and Engineering*, *21*(4). http://ijmse.iust.ac.ir/article-1-3784-en.html
10. Hajiebrahimi, M., Alamdari, S., Mirzaee, O., & Tajally, M. (2022). Luminescence investigation of Ce doped ZnO/$CdWO_4$ nanocomposite. Advanced Ceramics Progress, 8(3), 8-12. https://doi.org/10.30501/acp.2022.363264.1102.
11. Hajiebrahimi, M., Alamdari, S., Mirzaee, O., Albov, D., & Hvizdos, P. (2025). Flexible cerium-doped tungstate oxide/titanium dioxide nanocomposite for high-sensitivity energy conversion in optical applications. *Journal of Materials Science: Materials in Electronics*, *36*(2), 103. https://doi.org/10.1007/s10854-024-14141-8
12. Kannan, S., Subiramaniyam, N. P., & Sathishkumar, M. (2020). Effect of annealing temperature and Mn doping on the structural and optical properties of ZnS thin films for enhanced photocatalytic degradation under visible light irradiation. Inorganic Chemistry Communications, 119, 108068. https://doi.org/10.1016/j.inoche.2020.108068
13. Kim, M. R., Kang, Y. M., & Jang, D. J. (2007). Synthesis and characterization of highly luminescent CdS@ ZnS core– shell nanorods. The Journal of Physical Chemistry C, 111(50), 18507-18511. https://doi.org/10.1021/jp075218n
14. Li, B., & Wang, Y. (2011). Synthesis, microstructure, and photocatalysis of ZnO/CdS nano-heterostructure. Journal of Physics and Chemistry of Solids, 72(10), 1165-1169. https://doi.org/10.1016/j.jpcs.2011.07.010
15. Li, F., Jiang, Y., Hu, L., Liu, L., Li, Z., & Huang, X. (2009). Structural and luminescent properties of ZnO nanorods and ZnO/ZnS nanocomposites. Journal of alloys and compounds, 474(1-2), 531-535. https://doi.org/10.1016/j.jallcom.2008.06.149
16. Li, L., Daou, T. J., Texier, I., Kim Chi, T. T., Liem, N. Q., & Reiss, P. (2009). Highly luminescent CuInS2/ZnS core/shell nanocrystals: cadmium-free quantum dots for in vivo imaging. Chemistry of Materials, 21(12), 2422-2429. https://doi.org/10.1021/cm900103b
17. Li, Q., Meng, H., Zhou, P., Zheng, Y., Wang, J., Yu, J., & Gong, J. (2013). Zn1–x Cd x S solid solutions with controlled bandgap and enhanced visible-light photocatalytic H2-production activity. Acs Catalysis, 3(5), 882-889. https://doi.org/10.1021/cs4000975
18. Li, X., Wang, P., Huang, B., Qin, X., Zhang, X., Zhang, Q., ... & Dai, Y. (2017). Precisely locate Pd-Polypyrrole on TiO2 for enhanced hydrogen production. International Journal of Hydrogen Energy, 42(40), 25195-25202. https://doi.org/10.1016/j.ijhydene.2017.08.153
19. Luo, Z., Zhao, X., Zhang, H., & Jiang, Y. (2019). Zn0. 3Cd0. 7S nanorods loaded with noble-metal-free Ni3C co-catalyst enhancing photocatalytic hydrogen evolution. Applied Catalysis A: General, 582, 117115. https://doi.org/10.1016/j.apcata.2019.117115
20. Madhavi, J., Prasad, V., Reddy, K. R., Reddy, C. V., & Raghu, A. V. (2021). Facile synthesis of Ni-doped ZnS-CdS composite and their magnetic and photoluminescence properties. *Journal of Environmental Chemical Engineering*, *9*(6), 106335. https://doi.org/10.1016/j.jece.2021.106335
21. Malik, M. A., O'Brien, P., & Revaprasadu, N. (2002). A simple route to the synthesis of core/shell nanoparticles of chalcogenides. Chemistry of Materials, 14(5), 2004-2010. https://doi.org/10.1021/cm011154w
22. Mangla, D., Abbasi, A., Aggarwal, S., Manzoor, K., Ahmad, S., & Ikram, S. (2019). Effective removal of “non-biodegradable” pollutants from contaminated water. *Metal oxide-based photocatalyst for the degradation of organic pollutants in water*, 159. https://www.researchgate.net/publication/346426091
23. Mumin, M. A., Moula, G., & Charpentier, P. A. (2015). Supercritical CO 2 synthesized TiO 2 nanowires covalently linked with core–shell CdS–ZnS quantum dots: enhanced photocatalysis and stability. RSC Advances, 5(83), 67767-67779. https://doi.org/10.1039/C5RA08914J
24. Nizamoglu, S., Ozel, T., Sari, E., & Demir, H. V. (2007). White light generation using CdSe/ZnS core–shell nanocrystals hybridized with InGaN/GaN light emitting diodes. Nanotechnology, 18(6), 065709. https://doi.org/10.1088/0957-4484/18/6/065709

25. Pei, L., Liu, J., Xu, Y., Han, Y., Wu, J., Wang, Z., & Zhang, X. (2019). Hierarchical Zn1-xCdxS microclusters with superior visible-light-driven photocatalytic hydrogen generation performance. Journal of Alloys and Compounds, 809, 151869. https://doi.org/10.1016/j.jallcom.2019.151869

26. Reiss, P., Protiere, M., & Li, L. (2009). Core/shell semiconductor nanocrystals. small, 5(2), 154-168. https://doi.org/10.1002/smll.200800841

27. Schattka, J. H., Shchukin, D. G., Jia, J., Antonietti, M., & Caruso, R. A. (2002). Photocatalytic activities of porous titania and titania/zirconia structures formed by using a polymer gel templating technique. Chemistry of Materials, 14(12), 5103-5108. https://doi.org/10.1021/cm021238k

28. Shuai, X. M., & Shen, W. Z. (2011). A facile chemical conversion synthesis of ZnO/ZnS core/shell nanorods and diverse metal sulfide nanotubes. The Journal of Physical Chemistry C, 115(14), 6415-6422. https://doi.org/10.1021/jp2005716

29. Soltani, N., Saion, E., Hussein, M. Z., Erfani, M., Abedini, A., Bahmanrokh, G., ... & Vaziri, P. (2012). Visible light-induced degradation of methylene blue in the presence of photocatalytic ZnS and CdS nanoparticles. International journal of molecular sciences, 13(10), 12242-12258. https://doi.org/10.3390/ijms131012242

30. Suárez, P. L., García-Cortés, M., Fernández-Argüelles, M. T., Encinar, J. R., Valledor, M., Ferrero, F. J., ... & Costa-Fernández, J. M. (2019). Functionalized phosphorescent nanoparticles in (bio) chemical sensing and imaging–a review. Analytica chimica acta, 1046, 16-31. https://doi.org/10.1016/j.aca.2018.08.018

31. Yang, H., Huang, C., Su, X., & Tang, A. (2005). Microwave-assisted synthesis and luminescent properties of pure and doped ZnS nanoparticles. Journal of Alloys and Compounds, 402(1-2), 274-277. https://doi.org/10.1016/j.jallcom.2005.04.150

32. Yuan, Y. J., Chen, D., Yu, Z. T., & Zou, Z. G. (2018). Cadmium sulfide-based nanomaterials for photocatalytic hydrogen production. Journal of Materials Chemistry A, 6(25), 11606-11630. https://doi.org/10.1039/C8TA00671G

33. Yuan, Y. J., Li, Z., Wu, S., Chen, D., Yang, L. X., Cao, D., ... & Zou, Z. G. (2018). Role of two-dimensional nanointerfaces in enhancing the photocatalytic performance of 2D-2D MoS2/CdS photocatalysts for H2 production. Chemical Engineering Journal, 350, 335-343. https://doi.org/10.1016/j.cej.2018.05.172

34. Zhai, X., Zhang, R., Lin, J., Gong, Y., Tian, Y., Yang, W., & Zhang, X. (2015). Shape-controlled CdS/ZnS core/shell heterostructured nanocrystals: synthesis, characterization, and periodic DFT calculations. Crystal Growth & Design, 15(3), 1344-1350. https://doi.org/10.1021/cg501747e

35. Zhang, J., Xiao, M., Liu, Z., Han, B., Jiang, T., He, J., & Yang, G. (2004). Preparation of ZnS/CdS composite nanoparticles by coprecipitation from reverse micelles using CO2 as antisolvent. Journal of colloid and interface science, 273(1), 160-164. https://doi.org/10.1016/j.jcis.2004.02.032

36. Zhang, L., Jiang, D., Irfan, R. M., Tang, S., Chen, X., & Du, P. (2019). Highly efficient and selective photocatalytic dehydrogenation of benzyl alcohol for simultaneous hydrogen and benzaldehyde production over Ni-decorated Zn0. 5Cd0. 5S solid solution. Journal of energy chemistry, 30, 71-77. https://doi.org/10.1016/j.jechem.2018.03.014

37. Zhang, R., Xie, J., Wang, C., Liu, J., Zheng, X., Li, Y., ... & Su, B. L. (2017). Macroporous ZnO/ZnS/CdS composite spheres as efficient and stable photocatalysts for solar-driven hydrogen generation. Journal of Materials Science, 52, 11124-11134. https://doi.org/10.1007/s10853-017-1130-6

38. Zhou, X., Zhang, N., Yin, L., Zhao, Y., & Zhang, B. (2020). Few-layered WS2 nanosheets onto 1D CdS@ ZnCdS as efficient visible-light photocatalyst for hydrogen evolution. Ceramics International, 46(16), 26100-26108. https://doi.org/10.1016/j.ceramint.2020.07.105